Europe PMC Funders Group
Author Manuscript
Nat Cell Biol. Author manuscript; available in PMC 2006 October 09.

Published in final edited form as:
Nat Cell Biol. 2005 January ; 7(1): 48–55. doi:10.1038/ncb1206.

Coupling of ER exit to microtubules through direct interaction of COPII with dynactin

Peter Watson[1,3], **Rebecca Forster**[2,3], **Krysten J. Palmer**[1], **Rainer Pepperkok**[2,4], and **David J. Stephens**[1,4]

[1]Department of Biochemistry, University of Bristol, School of Medical Sciences, University Walk, Bristol BS8 1TD, UK.

[2]Cell Biology and Biophysics Programme, EMBL, Meyerhofstrasse 1, D-69117 Heidelberg, Germany.

Abstract

Transport of proteins from the endoplasmic reticulum (ER) to the Golgi is mediated by the sequential action of two coat complexes: COPII concentrates cargo for secretion at ER export sites, then COPI is subsequently recruited to nascent carriers and retrieves recycling proteins back to the ER. These carriers then move towards the Golgi along microtubules, driven by the dynein/dynactin complexes. Here we show that the Sec23p component of the COPII complex directly interacts with the dynactin complex through the carboxy-terminal cargo-binding domain of $p150^{Glued}$. Functional assays, including measurements of the rate of recycling of COPII on the ER membrane and quantitative analyses of secretion, indicate that this interaction underlies functional coupling of ER export to microtubules. Together, our data suggest a mechanism by which membranes of the early secretory pathway can be linked to motors and microtubules for subsequent organization and movement to the Golgi apparatus.

The COPII complex cycles between the cytosol and discrete sites on the ER membrane1. Directed assembly of COPII on the ER membrane is initiated by GDP/GTP exchange on the small GTPase Sar1p, catalysed by Sec12p2. This results in the sequential recruitment of two binary complexes, Sec23p–Sec24p and Sec13p–Sec31p3. Sec23p–Sec24p acts as a GTPase-activating protein for Sar1p as well as having a direct role in cargo binding2. Sec13p–Sec31p provides the structural scaffold for membrane deformation and vesicle formation2. ER-to-Golgi transport in mammalian cells proceeds by concentration of cargo into COPII-coated ER export sites (ERES)2, followed by formation of vesicular–tubular transport carriers (VTC)4,5, which then move in a COPI-dependent4 and dynein/dynactin-dependent6 manner along microtubule tracks towards the Golgi. The movement of membranes along cytoskeletal tracks largely determines the directionality and efficiency of membrane traffic in mammalian cells. The microtubule and actin cytoskeletons coordinate many membrane traffic processes7, notably the movement of post-Golgi membranes, endosomes and retrograde transport carriers. There is considerable evidence for microtubules functioning in cargo export from the ER and subsequent VTC motility. ERES align along microtubules in certain cell types8, Golgi-directed VTCs localize along a population of stable microtubules9,10 and translocate along microtubules towards the Golgi in a dynactin-

[4]Correspondence should be addressed to D.J.S. (david.stephens@bristol.ac.uk) or R.P. (pepperko@embl-heidelberg.de).
[3]These authors contributed equally to this work.

Note: Supplementary Information is available on the Nature Cell Biology website.

COMPETING FINANCIAL INTERESTS
The authors declare that they have no competing financial interests.

Europe PMC Funders Author Manuscripts
Europe PMC Funders Author Manuscripts

Europe PMC Funders Author Manuscripts

Europe PMC Funders Author Manuscripts

dependent manner6, and the plus-end-directed motor protein kinesin has been shown to localize to ERES *in vitro*11 and to pre-Golgi intermediates (VTCs) *in vivo*12. However, little is known about the mechanisms that couple membranes of the early secretory pathway to microtubules. How is the localization of COPII to discrete sites generated and maintained? How are VTCs linked to microtubules, and how is motility of VTCs regulated?

ERES undergo predominantly short- but also long-range movements in mammalian cells that are completely inhibited following depolymerization of microtubules13,14. Imaging of live cells labelled with yellow fluorescent protein (YFP)–Sec23Ap15 and rhodamine-tubulin showed that the majority of ERES localized in the vicinity of microtubules (Fig. 1a). Time-lapse analysis showed that dynamic microtubules frequently repolymerized along trajectories that passed one or more ERES (Fig. 1a and see Supplementary Information, Movie 1, enlarged in Fig. 1b). The association of ERES with microtubules persisted for at least several minutes (Fig. 1a and see Supplementary Information, Movie 1, enlarged in Fig. 1b). These data suggest that a significant fraction of growing microtubules are targeted towards ERES and are consistent with a 'search-and-capture' mechanism for the targeting of growing microtubules to endomembranes16. To obtain more direct evidence for this we tested the targeting of growing microtubules using green fluorescent protein (GFP)-labelled plus-end tracking proteins (+TIPs)17. Figure 1c (and see Supplementary Information, Movies 2 and 3) shows that GFP– $p150^{Glued}$ (ref. 16) labels the plus ends of microtubules in HeLa cells (Fig. 1c, arrow) and that these structures migrate towards and through ERES labelled with GFP–Sec23Ap (Fig. 1c, arrowhead, and see Fig. 1d). We obtained identical data using an alternative +TIP–GFP–end-binding protein 1 (GFP–EB1)18 (data not shown).

To extend these observations, we measured the association of newly polymerized microtubules with ERES following incubation with and subsequent washout of nocodazole. Consistent with the data presented in Fig. 1, newly polymerizing microtubules become rapidly associated with ERES after nocodazole washout (Fig. 2a). Newly polymerized microtubules associated more frequently with COPII when compared with either γ-adaptin-positive structures or peroxisomes (data not shown). Analyses of fixed and immunostained cells confirmed these observations with endogenous proteins (data not shown). Injection of anti-EAGE (a function blocking antibody directed against the COPI complex19), or of $Sar1p^{(H79G)}$ (a dominant negative mutant that inhibits COPII5), reduced the number of microtubules that had at least one associated ERES, compared with controls (Fig. 2a, b). Inactivation of COPII and COPI function also reduced the number of ERES associated with at least one microtubule (Fig. 2a, c). These data imply that a functional early secretory pathway is required for the association of ERES with microtubules.

These data support the hypothesis that association of membranes and microtubules is initiated at an early, COPII-dependent stage of ER-to-Golgi transport. We therefore set out to identify COPII-interacting molecules as potential mediators of the association of ERES with microtubules. Two-hybrid screening with Sec23Ap identified one positive clone encoding a C-terminal fragment of $p150^{Glued}$ (amino acids 938–1254, consequently named CT^{Glued}). $p150^{Glued}$ is a component of the dynactin complex that interacts with the dynein motor20 and also binds microtubules21. This clone was found to specifically interact with Sec23Ap but not lamin (Fig. 3a). Further assays showed that CT^{Glued} also interacts with Sec24Dp but not with Sec13p or Sec31Ap (Fig. 3a). A direct interaction between Sec23Ap and $p150^{Glued}$ was demonstrated using surface plasmon resonance (SPR) and 'glutathione *S*-transferase (GST) pull-down' experiments. Figure 3b shows that an interaction was detectable with GST–CT^{Glued} (black trace) but not with GST alone (grey). Figure 3c shows the averaged binding of His_6-hSec23Ap to GST–CT^{Glued} compared with GST from six representative SPR experiments of which one is shown in Fig. 3b. Binding of His_6-hSec23Ap to GST–CT^{Glued} is only very weakly detectable with binding profiles indicative

Europe PMC Funders Author Manuscripts

Europe PMC Funders Author Manuscripts

of a very fast off-rate. We were also able to demonstrate binding of His_6-Sec23Ap to immobilized GST–CT^{Glued} (Fig. 3d, lane 2) confirming that this interaction is direct. Sec23Ap interacted with $p150^{Glued}$ by co-immunoprecipitation from HeLa cell lysates (Fig. 3e). Antibodies specific for Sar1p could also immunoprecipitate $p150^{Glued}$ (Fig. 3f). This was less efficient than immunoprecipitation of $p150^{Glued}$ with anti-Sec23Ap antibodies, probably owing to the transient nature of COPII complex assembly22 (and see Supplementary Information, Table 1). The interaction is specific to Sec23Ap because we were unable to co-immunoprecipitate $p150^{Glued}$ with antibodies specific to either Sec31Ap23 or β′-COP24 (of the COPI complex) (Fig. 3f). The lower panels of Fig. 3f show that the antibodies used for immunoprecipitation are effective in immunoprecipitation of their targets. Furthermore, we found that overexpression of a cyan fluorescent protein (CFP)-tagged form of CT^{Glued} in HeLa cells prior to lysis and immunoprecipitation resulted in a decrease in the amount of $p150^{Glued}$ that could be immunoprecipitated with anti-Sec23Ap but not by anti-$p50^{dynamitin}$ (Fig. 3g).

Immunofluorescence staining of fixed cells revealed limited but definite colocalization of COPII and $p150^{Glued}$ (Fig. 4a, b). Eight per cent (± 1.7%) of COPII structures within any one cell colocalized with $p150^{Glued}$ (>1,000 Sec23Ap-labelled structures analysed). In contrast, only 2.9% (± 0.28%) of γ-adaptin-positive structures (clearly defined puncta in the periphery of cells) colocalized with $p150^{Glued}$ (>800 γ-adaptin-positive structures analysed). A similar degree of colocalization was seen with two different anti-$p150^{Glued}$ monoclonal antibodies (Fig. 4a, b) and one polyclonal16 (data not shown). This of course reflects the distribution of these proteins at the instant at which the cells were fixed. In addition to the predominant localization of $p150^{Glued}$ to plus ends, there will also be a soluble pool in these cells, but this is largely extracted by methanol fixation. We do not detect significant punctate labelling of $p150^{Glued}$ throughout the cell, other than at microtubule plus ends. We have observed a similar association of structures that label with antibodies directed against dynein heavy chain 1a, at or adjacent to COPII-labelled structures (data not shown). Intriguingly, on depolymerization of microtubules with nocodazole for 10 or 30 min (depolymerization of microtubules being confirmed by immunofluorescence with anti-α-tubulin antibodies (data not shown)) a population of $p150^{Glued}$ localized in the direct vicinity of ERES (Fig. 4c, d, arrowheads in d). This may represent binding of dynactin to newly formed VTCs and, in these experiments, we cannot discriminate between direct recruitment to VTCs and COPII-dependent recruitment.

The data presented above suggest the presence of a protein interaction network that functions to coordinate vesicle generation with subsequent VTC formation and transport. We therefore measured the rate of turnover of COPII components on the ER membrane using fluorescence recovery after photobleaching (FRAP; see Supplementary Information, Methods and Fig. S1). Overexpression of either $p150^{Glued}$ or CFP–CT^{Glued} caused similar changes to the rate of recycling of both Sec23Ap ($t_{½}$ decreased from 4.0 ± 0.3 s to 1.6 ± 0.4 s in cells expressing CT^{Glued}) and Sec31Ap ($t_{½}$ decreased from 3.1 ± 0.1 s to 1.5 ± 0.3 s) compared with control cells (see Supplementary Information, Table 1). Similar data were obtained with Sec24Dp and Sec13p (data not shown). Microinjection of $p50^{dynamitin}$ also substantially accelerated the turnover of these COPII components. Depolymerization of microtubules had little effect on the steady state distribution of COPII14 (Fig. 4). However, turnover at single ERES of both Sec23Ap and Sec31Ap was significantly accelerated following depolymerization of microtubules with nocodazole (t½ decreased from 4.0 ± 0.3 s to 2.6 ± 0.2 s for Sec23Ap and from 3.1 ± 0.1 s to 1.9 ± 0.4 s for Sec31Ap, see Supplementary Information, Table 1).

Disruption of COPII function would be expected to have an effect on cargo export from the ER. We therefore examined the effects of expression of CFP–CT^{Glued} on export from the

Europe PMC Funders Author Manuscripts

Europe PMC Funders Author Manuscripts

ER of the widely used secretory cargo ts045-G from the ER by time-lapse microscopy4,6,14. Figure 5a shows multiple panels taken from Supplementary Movie 4 (enlarged in Fig. 5b, see Supplementary Information, Movie 5). In control (CFP-expressing) cells, a substantial fraction of the expressed ts045-G–GFP reaches the Golgi within 5 min (300 s, arrowheads). In contrast, it is not until 15 min (900 s, arrowhead) that a similar quantity of ts045-G–GFP in the Golgi of cells expressing CFP–CT^{Glued} can be seen. Indeed in the earlier frames from this sequence (0–600 s, see Supplementary Information, Movies 4 and 5), it becomes clear that there is a defect in the formation of punctate, ts045-G–GFP-containing transport carriers (Fig. 5b). In CFP-transfected cells, 4 min after a shift to 32 °C (1 min after the start of imaging), on average 23 ± 8 punctate structures were observed. In cells transfected with CFP–CT^{Glued}, only 3 ± 3 punctate structures could be observed. At 8 min after release of the temperature block (5 min of imaging), this difference was less pronounced, with an average of 45 ± 12 punctate structures in control cells and 29 ± 10 structures in CFP–CT^{Glued}-expressing cells (n = 10 cells for each condition). Quantification of the proportion of total transport of ts045-G to the plasma membrane shows that CFP–CT^{Glued} significantly inhibits transport to the plasma membrane (Fig. 5c). These data show that the delay in transport is perpetuated through the secretory pathway.

It is possible that these defects result from direct disruption of the dynactin complex. However, these data are different from those seen on expression of $p50^{dynamitin}$ (ref. 6). Critically, $p50^{dynamitin}$ results in an accumulation of cargo in punctate structures (ERES and VTCs)6, but CT^{Glued} inhibits any such accumulation at ERES, and cargo export from the ER is delayed (Fig. 5). The velocities of VTCs identified in these time-lapse movies were measured using particle tracking. Average velocities of VTCs were 1.21 ± 0.34 μm s^{-1} in CFP-transfected cells and 1.24 ± 0.30 μm s^{-1} in CFP–CT^{Glued}-transfected cells. Figure 5d shows a histogram of the average velocity of these VTCs along with the scatter of individual measurements. We conclude from this that there is no difference in VTC velocity in these two experiments. It is possible that overexpression of CFP–CT^{Glued} mimics the effects of $p50^{dynamitin}$ and inhibits traffic through functional disruption of dynactin structure (that is, uncoupling of the side arm from the central domain of dynactin25,26). Sedimentation analyses reveal that this is not the case (see Supplementary Information, Fig. S2). These data show that expression of CFP–CT^{Glued} acts by a mechanism distinct to that of $p50^{dynamitin}$, most probably through inhibition of the Sec23Ap–$p150^{Glued}$ interaction (see also Fig. 3g). Furthermore, overexpression of dynactin components, such as $p50^{dynamitin}$, causes a variety of defects including disorganization of microtubules and Golgi fragmentation27. Expression of CT^{Glued} did not cause these effects (see Supplementary Information, Fig. S3), consistent with a defect in one or more aspects of ER-to-Golgi transport, but not with gross defects in Golgi organization.

The experiments described here suggest that the association of ERES with microtubules is mediated directly or indirectly by the dynactin complex. We have shown that ERES rapidly associate with newly polymerized microtubules, the tips of which carry $p150^{Glued}$ [28]. One could envisage that these newly polymerizing microtubules grow in close enough proximity to ERES for this to act as a mechanism of targeted delivery of $p150^{Glued}$ to ERES, or indeed in capture of microtubules by ERES, which already have $p150^{Glued}$. The interaction of COPII with dynactin is consistent with previous findings16 showing a role for the regulated binding of dynactin to newly formed transport carriers emerging from the ER. It is conceivable that a pool of dynactin localizes to ERES when it is associated along the length, rather than with the tips of microtubules. Our data suggest that an intact microtubule cytoskeleton is not required for recruitment of $p150^{Glued}$ to ERES, thus dynactin may be recruited to ERES from cytosol. Not enough is known about the dynamics of $p150^{Glued}$ at plus ends, or indeed along the rest of the microtubule length, to define this further. The number of COPII–dynactin ‘capture’ events happening at an ERES (which in a typical ~1

Europe PMC Funders Author Manuscripts

Europe PMC Funders Author Manuscripts

μm area of membrane is potentially high) means that the association of these sites with microtubules is maintained.

We have shown that $p150^{Glued}$ can interact, albeit weakly, with partially assembled COPII (the pre-budding complex of Sar1p and Sec23p). We cannot detect an interaction between Sec31p and $p150^{Glued}$, but we cannot conclusively define whether this is owing to the rapid dissociation of assembled COPII22, an inability of our antibodies to detect an association, or because $p150^{Glued}$ does not associate with fully assembled COPII. The association of dynactin with COPII is transitory in nature as dynactin is then 'transferred' to the nascent VTC where it is probably anchored by another dynactin receptor such as spectrin, which is known to anchor dynactin on Golgi membranes29. Because VTCs are coated with COPI30 *en route* to the Golgi but not with COPII13,14, there are likely to be alternative binding partners for $p150^{Glued}$, or other components of the dynactin or dynein complexes, to mediate subsequent transport. Monitoring the turnover of COPII components at ERES suggests that an intact dynactin complex serves to stabilize the COPII coat on the membrane. Stable association of COPII with membranes and functional coupling to microtubules is likely to be a precursor to productive budding events in living cells. We show that $p50^{dynamitin}$ expression disrupts the dynactin complex and should thus interfere with both $p50^{dynamitin}$ and $p150^{Glued}$ function; in contrast, CT^{Glued} expression does not seem to disrupt the dynactin complex and should not directly interfere with $p50^{dynamitin}$ function. On the basis of these results we conclude that the changes in COPII dynamics seen with CT^{Glued} expression are due to the inhibited interaction of $p150^{Glued}$ with Sec23p. Thus, expression of CT^{Glued} inhibits export of cargo from the ER, but not the motility of VTCs once they have formed, consistent with a role for dynactin at an early stage of COPII function.

Most ERES themselves are relatively immobile13,14 and, despite rapid recycling of COPII components on and off the ER membrane, are in fact very stable structures14. The interaction of COPII with dynactin therefore supports a role for COPII in the generation of membrane domains to which machinery such as dynactin, dynein, Rabs31, tethers31 and SNAREs32,33 can be recruited in advance of their requirement. This would increase the efficiency of a complex process, including vesicle formation, microtubule membrane interactions and activity of motors, that needs to be tightly regulated in space and time. In conclusion, we have identified a direct link between the ER export machinery and the microtubule cytoskeleton. These data provide a molecular mechanism linking cargo export from ER exit sites to microtubules for dynein-dependent, directional transport to the Golgi.

METHODS

Materials

Nocodazole was from Merck Biosciences (Nottingham, UK); plasmids encoding YFP–Sec23Ap and CFP–Sec24Dp (where A and D denote the isoforms of these proteins) are described in ref. 15; Sec31Ap was a gift from F. Gorelick (Yale, USA) and was transferred from pCR2.1 vectors into pECFP-C1 and pEYFP-C1 vectors (Clontech, Palo Alto, CA) using flanking EcoR1 sites. cDNA encoding YFP–PMP4, a peroxisomal marker, was a gift from J. Simpson (EMBL, Heidelberg, Germany); cDNA encoding $p50^{dynamitin}$ (ref. 25), recombinant $p50^{dynamitin}$ and rhodamine-tubulin were gifts from I. Vernos (EMBL, Heidelberg); chick $p150^{Glued}$ and $p50^{dynamitin}$ were gifts from T. Schroer (Johns Hopkins, Baltimore, MD); polyclonal anti-Sec31p was a gift from W. Hong (IMCB, Singapore); anti-VG and YFP–ts-045-G were from K. Simons (MPI-CBG, Dresden, Germany); monoclonal anti-α-tubulin (DM1A) was from Neomarkers (Fremont, CA); EAGE is described in ref. 21; anti-Sec23Ap was from Affinity Bioreagents (Golden, CO); anti-DHC1a was provided by V. Allan (University of Manchester, UK); and anti-BSTR has been described previously24. Monoclonal antibodies directed against $p50^{dynamitin}$ (611003) and $p150^{Glued}$ (610474 and

Europe PMC Funders Author Manuscripts

Europe PMC Funders Author Manuscripts

612709) were from Pharmingen (San Diego, CA); antibodies against γ-adaptin were from BD Biosciences (San Jose, CA); and rabbit and mouse IgG were from Sigma (St Louis, MO). PtK2 cells stably expressing YFP–α-tubulin were a gift from P. Keller (MPI-CBG, Dresden, Germany). GFP–$p150^{Glued}$ and a polyclonal anti-$p150^{Glued}$ antibody were provided by K. Vaughan (Notre Dame, USA). GFP–EB1 was from E. Morrison (Leeds, UK).

Cell culture and microinjection

HeLa cells (ATCC CCL-2) and Vero cells (ATCC CCL-81) were grown on live cell dishes (MatTek, Ashland, MA) or 22-mm coverslips in DMEM (Life Technologies, Karlsruhe, Germany) supplemented with 10% FCS, 1% penicillin and streptomycin, and 1% glutamine. For microinjection, cells were plated 48 h in advance. For live cell imaging, plasmid encoding YFP–Sec23Ap (15 ng μl^{-1}) was microinjected and expressed for 16 h. Rhodamine-tubulin was diluted to 5 $\mu g\ ml^{-1}$ in ice-cold injection buffer (5 mM sodium phosphate, 100 mM KCl, pH 7.3), centrifuged at 4 °C and subsequently injected into expressing cells. Cells were left to incubate for several hours before imaging to ensure incorporation into microtubules. Recombinant $p50^{dynamitin}$ (5 mg ml^{-1}), EAGE (1 mg ml^{-1}) or rabbit IgG (1 mg ml^{-1}) were co-injected with 0.03 mg ml^{-1} rhodamine dextran (Sigma) and left to incubate for 1 h. Plasmids encoding $Sar1^{H79G}$, $p150^{Glued}$, $p50^{dynamitin}$ and CFP–CT^{Glued} were co-injected with a plasmid expressing YFP–Sec23Ap, and left to express for 16 h.

Microtubule repolymerization and quantification of colocalization

Vero cells were microinjected with constructs encoding YFP–Sec23Ap for 16–18 h, and microinjected with 1 mg ml^{-1} rabbit IgG or 1 mg ml^{-1} EAGE, each with a co-injection marker of 0.03 mg ml^{-1} rhodamine-dextran. $Sar1p^{(H79G)}$ inhibition was achieved by co-expression from a plasmid. Cells were then treated with 10 μM nocodazole for 1 h at 37 °C. Nocodazole was then washed out using pre-warmed medium. Cells were then incubated at 37°C for 3 min, fixed, and stained for endogenous α-tubulin. Images of stained cells were acquired with a Zeiss (Thornwood, NY) microscope system equipped with a cooled CCD (charge-coupled device) camera (Cell Observer). The tubulin and COPII images were separated and individual randomly selected centrosomal microtubules were highlighted with an overlay that was superimposed onto the COPII image using IPLab software package (Scanalytics, Fairfax, VA). Association of microtubules with ERES was defined as being observed when the microtubule overlay was in contact with COPII-labelled ERES. COPII-coated ERES in close vicinity to microtubules were not counted as associated (see Fig. 2a, c for examples). The percentage of the microtubules associated with at least one ERES and the percentage of ERES associated with at least one microtubule (Fig. 2) was determined and the data normalized to the values obtained in unperturbed control cells (set as 100%). In all experiments, at least 10 cells were measured for each condition. Identical results were obtained in living cells expressing YFP–α-tubulin and YFP–Sec23Ap (data not shown).

Live cell imaging of microtubules and COPII

Vero cells were treated as above. Cells were either untreated or subjected to the repolymerization assay described above. Immediately after washout of nocodazole, cells were imaged in pre-warmed carbonate free imaging medium, at 37 °C, using an Ultraview RS imaging system (Perkin Elmer, Wellesley, MA), fitted with argon (488 nm) and argon/krypton (568 nm) ion lasers, with ×100 1.3 N.A. oil immersion objective (Carl Zeiss, Jena, Germany). Images were acquired continuously, with intervals between frames of 0.8 s. Channels were acquired sequentially, using 50% laser power.

Europe PMC Funders Author Manuscripts

Europe PMC Funders Author Manuscripts

Immunofluorescence and microscopy

Living cells were imaged as previously described14. For immunofluorescence, cells were fixed with methanol at −20 °C for 4 min and processed as described14. HeLa, Vero or PtK2 cells were imaged using an Olympus/TILL Photonics imaging system as described15, Leica TCS-NT upright confocal microscope or Leica TCS-SP2 AOBS confocal microscope. Images were processed using Photoshop 6.0 (Adobe, Uxbridge, UK), ImageJ (http://rsb.info.nih.giv.ij) and QuickTime Pro (Apple, Cupertino, CA). Montages were generated using Adobe Illustrator 10 (Adobe). Movies were compiled in QuickTime Pro using 'Photo JPEG' compression.

FRAP

For FRAP experiments, Vero cells were microinjected with 15 ng μl^{-1} constructs encoding CFP–Sec31Ap and Sec23Ap, CFP–Sec24Dp or YFP–Sec23Ap, or CFP–Sar1p and YFP–Sec23Ap, as above. A full description of FRAP methods used is available as Supplementary Information.

Two-hybrid library screening

A human adult brain two-hybrid library (Clontech, Oxford, UK) was screened using human Sec23Ap as bait by yeast mating using the Matchmaker III system. Independent clones (2×10^6) were screened, positive clones isolated and interaction confirmed by retransformation and analysis using negative control constructs as described in the text. Putative positives were identified by DNA sequencing. Positive interactions were confirmed using both α-gal and β-gal colorimetric assays.

Immunoprecipitation

HeLa cells were grown to 90% confluence, lysed in RIPA buffer (50 mM Tris-HCl pH 7.4, 150 mM NaCl, 1% Triton X-100, 0.5% sodium deoxycholate, 0.1% SDS, protease inhibitor cocktail (Calbiochem, Nottingham, UK)) and subjected to immunoprecipitation with primary antibodies, followed by incubation with GammaBind-G sepharose (Amersham Biosciences, Chalfont St Giles, UK). Complexes were washed three times for 5 min each in RIPA followed by SDS–PAGE and immunoblotting. Proteins were separated using 3–8% Tris-acetate or 4–12% Bis-Tris gels (Invitrogen, Carlsbad, CA) and transferred to PVDF membranes. Blots were developed using chemiluminescent detection (Roche, Lewes, UK). For the experiments shown in Fig. 3f, cells were lysed in 50 mM Tris-HCl pH 7.4, 100 mM NaCl, 1% Triton X-100 with protease inhibitor cocktail; blots in Fig. 3f were developed using SuperSignal West Femto chemiluminescent substrate (Pierce/Perbio, Cramlington, UK).

Protein expression and purification

The two-hybrid clone corresponding to the C terminus of $p150^{Glued}$ was cloned into pGEX4T2 (Amersham Pharmacia Biotech, Cardiff, UK). GST–CT^{Glued} and GST were expressed and purified according to the manufacturer's standard protocols. The coding region of human Sec23Ap was cloned into pFastBac-HTa (Invitrogen). Recombinant bacmids were generated and transfected into Sf9 cells. Viruses were collected, amplified and used for expression in Sf9 cells. Cells were lysed in lysis buffer (50 mM Tris-HCl pH 7.4, 150 mM NaCl, 1% Triton X-100, 0.5% sodium deoxycholate, complete protease inhibitors (Roche, Lewes, UK)) and purified using Talon metal affinity chromatography (Clontech) according to manufacturers' protocols.

Europe PMC Funders Author Manuscripts

Europe PMC Funders Author Manuscripts

Direct binding assays

Binding analysis was performed using bacterially expressed GST and GST–CT^{Glued} was purified using glutathione-sepharose (Amersham Biosciences, Little Chalfont, UK) according to the manufacturer's instructions. His_6-Sec23Ap was purified from baculovirus-infected HighFive (Invitrogen) cells using Talon affinity resin (Clontech). Protein was eluted with 100 mM EDTA and used directly in the binding assay. Binding was measured by surface plasmon resonance using a Biacore 1000 system (Biacore, Uppsala, Sweden) at a flow rate of 10 μl min^{-1} and using phosphate-buffered saline as running buffer. An antibody to GST (Amersham Pharmacia Biotech, Piscataway, NJ) was immobilized on a CM5 dextran sensor chip (Biacore, Neuchâtel, Switzerland) using amine-coupling chemistry. Equal quantities (100 resonance units, RU) of GST or GST–CT^{Glued} were captured using anti-GST antibodies followed by measurement of interaction with His_6-hSec23Ap over 60 s. In control experiments, His_6-hSec23Ap did not show any binding to the dextran matrix directly or to the anti-GST antibody (data not shown). 'GST pull-down' experiments were performed by incubating 5 μg His_6-Sec23Ap with 5 μg of GST or GST–CT^{Glued} immobilized on glutathione sepharose for 2 h at 4 °C. Beads were then washed three times for 5 min each in PBS followed by boiling in SDS sample buffer, and SDS–PAGE and immunoblotting using an anti-Sec23Ap antibody.

ts045-G–GFP transport assay

For the quantitative transport assay, cells were transfected with plasmids encoding either CFP or CFP–CT^{Glued} along with one encoding ts045-G–YFP. Cells were incubated at 39.5 °C for 16 h before addition of HEPES pH 7.4 to a final concentration of 30 mM and incubation in a water bath at 32 °C for the times indicated. Transport of ts045-G–YFP to the plasma membrane was quantified using anti-VG immunofluorescence of non-permeabilized cells fixed with 3% paraformaldehyde. We measured the proportion or ts045-G–YFP at the plasma membrane after 60 min at 32 °C, compared with the total plasma membrane fluorescence after 90 min at 32 °C (found to be the same as total cellular YFP fluorescence; that is, the total amount of ts045-G–YFP expressed). Only those cells expressing CFP or CFP–CT^{Glued} in the range of 50–150 greyscale units on an 8-bit scale were quantified to eliminate those expressing either very high or barely detectable levels. After 90 min at 32 °C, total cellular fluorescence was equal to total plasma membrane fluorescence. Triplicate samples were analysed to determine the amount of plasma membrane ts045-G–YFP at 60 min and 90 min. The percentage transport at 60 min was then calculated for each of the three experiments. For live cell imaging, cells were transferred into pre-warmed (32 °C) imaging medium (MEM without phenol red, supplemented with 30 mM HEPES pH 7.4 and 0.1% sodium bicarbonate) and moved directly to the pre-heated microscope (heated using a Solent Scientific Perspex box (Segensworth, UK), with the heater set at 35 °C to maintain cells at 32 °C). Imaging then began as soon as possible, in reality at 3 min after the shift to 32 °C. Times given on the movies and associated still images are the time from the start of imaging. Particle identification and velocity tracking was done using Volocity version 2.5 (Improvision, Coventry, UK). Greater than 100 clearly definable VTCs (at least 20 from each of 5 different cells) were quantified from cells transfected with either CFP or CFP–CT^{Glued}. Movies were acquired within 10 min after the shift from 39.5 to 32 °C.

Sedimentation assay

Integrity of the dynactin complex was analysed by sucrose density sedimentation. The protocol was based on that of ref. 25. Cells grown in 100-mm dishes were incubated in 1 ml of sedimentation buffer (50 mM Tris-HCl pH 7.5, 150 mM NaCl, 1 mM EDTA, Complete Protease inhibitor cocktail) containing 1% NP-40 for 15 min at 4 °C. Cell lysates were centrifuged at 25,000*g* (Eppendorf 5417R) at 4 °C for 30 min and the supernatant was recovered. Sucrose gradients (10 ml of 5–20% sucrose in sedimentation buffer) were

prepared and 800 μl of each extract were carefully layered on top. The gradients were centrifuged in a TH-641 swing out rotor (Sorvall OTD65B Ultracentrifuge) at 96,330*g* for 18 h at 4 °C. 1-ml fractions were collected and 20 μl analysed by SDS–PAGE followed by western blotting with antibodies directed against $p50^{dynamitin}$ or $p150^{Glued}$. The antibody used for detection of $p50^{dynamitin}$ does not recognize the transfected chick $p50^{dynamitin}$ protein (transduction laboratory's data and our data, not shown).

BIND identifiers

Four BIND identifiers (www.bind.ca) are associated with this manuscript: 183944, 183945, 183946 and 183947.

Supplementary Material

Refer to Web version on PubMed Central for supplementary material.

Acknowledgments

We are grateful to H.-P. Hauri, K. Simons, J. Simpson, F. Gorelick, I. Vernos, P. Keller, K. Vaughan, T. Schroer and V. Allan for gifts of reagents, to A. Geerlof for help with baculovirus expression, to J. Konkel and B. Joggerst for technical assistance, and to G. Banting, H. Mellor and J. Lane for discussions and critical reading of the manuscript. Work within the Stephens laboratory was supported by the Medical Research Council (through a Research Career Development Award to D.J.S.), the Wellcome Trust and the Royal Society. The University of Bristol Cell Imaging Facility was funded by an Infrastructure Award and Joint Research Equipment Initiative Grant from the Medical Research Council. We also thank Perkin Elmer, Leica Microsystems, Olympus Europe and Carl Zeiss for support of the Advanced Light Microscopy Facility at EMBL, Heidelberg. R.F. was funded by the EMBL predoctoral student programme.

References

1. Orci L, et al. Mammalian Sec23p homologue is restricted to the endoplasmic reticulum transitional cytoplasm. Proc. Natl Acad. Sci. USA. 1991; 88:8611–8615. [PubMed: 1924322]
2. Barlowe C. COPII-dependent transport from the endoplasmic reticulum. Curr. Opin. Cell Biol. 2002; 14:417–422. [PubMed: 12383791]
3. Barlowe C, et al. COPII: a membrane coat formed by Sec proteins that drive vesicle budding from the endoplasmic reticulum. Cell. 1994; 77:895–907. [PubMed: 8004676]
4. Scales SJ, Pepperkok R, Kreis TE. Visualization of ER-to-Golgi transport in living cells reveals a sequential mode of action for COPII and COPI. Cell. 1997; 90:1137–1148. [PubMed: 9323141]
5. Aridor M, Bannykh SI, Rowe T, Balch WE. Sequential coupling between COPII and COPI vesicle coats in endoplasmic reticulum to Golgi transport. J. Cell Biol. 1995; 131:875–893. [PubMed: 7490291]
6. Presley JF, et al. ER-to-Golgi transport visualized in living cells. Nature. 1997; 389:81–85. [PubMed: 9288971]
7. Kamal A, Goldstein LS. Principles of cargo attachment to cytoplasmic motor proteins. Curr. Opin. Cell Biol. 2002; 14:63–68. [PubMed: 11792546]
8. Ralston E, Ploug T, Kalhovde J, Lomo T. Golgi complex, endoplasmic reticulum exit sites, and microtubules in skeletal muscle fibers are organized by patterned activity. J. Neurosci. 2001; 21:875–883. [PubMed: 11157074]
9. Saraste J, Svensson K. Distribution of the intermediate elements operating in ER to Golgi transport. J. Cell Sci. 1991; 100:415–430. [PubMed: 1808196]
10. Mizuno M, Singer SJ. A possible role for stable microtubules in intracellular transport from the endoplasmic reticulum to the Golgi apparatus. J. Cell Sci. 1994; 107:1321–1331. [PubMed: 7929638]
11. Aridor M, et al. The Sar1 GTPase coordinates biosynthetic cargo selection with endoplasmic reticulum export site assembly. J. Cell Biol. 2001; 152:213–229. [PubMed: 11149932]

Europe PMC Funders Author Manuscripts
Europe PMC Funders Author Manuscripts

Europe PMC Funders Author Manuscripts

Europe PMC Funders Author Manuscripts

12. Lippincott-Schwartz J, Cole NB, Marotta A, Conrad PA, Bloom GS. Kinesin is the motor for microtubule-mediated Golgi-to-ER membrane traffic. J. Cell Biol. 1995; 128:293–306. [PubMed: 7844144]
13. Hammond AT, Glick BS. Dynamics of transitional endoplasmic reticulum sites in vertebrate cells. Mol. Biol. Cell. 2000; 11:3013–3030. [PubMed: 10982397]
14. Stephens DJ, Lin-Marq N, Pagano A, Pepperkok R, Paccaud JP. COPI-coated ER-to-Golgi transport complexes segregate from COPII in close proximity to ER exit sites. J. Cell Sci. 2000; 113:2177–2185. [PubMed: 10825291]
15. Stephens DJ. *De novo* formation, fusion and fission of mammalian COPII-coated endoplasmic reticulum exit sites. EMBO Rep. 2003; 4:210–217. [PubMed: 12612614]
16. Vaughan PS, Miura P, Henderson M, Byrne B, Vaughan KT. A role for regulated binding of p150(Glued) to microtubule plus ends in organelle transport. J. Cell Biol. 2002; 158:305–319. [PubMed: 12119357]
17. Carvalho P, Tirnauer JS, Pellman D. Surfing on microtubule ends. Trends Cell Biol. 2003; 13:229–237. [PubMed: 12742166]
18. Askham JM, Vaughan KT, Goodson HV, Morrison EE. Evidence that an interaction between EB1 and p150(Glued) is required for the formation and maintenance of a radial microtubule array anchored at the centrosome. Mol. Biol. Cell. 2002; 13:3627–3645. [PubMed: 12388762]
19. Pepperkok R, et al. Beta-COP is essential for biosynthetic membrane transport from the endoplasmic reticulum to the Golgi complex *in vivo*. Cell. 1993; 74:71–82. [PubMed: 8334707]
20. Vaughan KT, Vallee RB. Cytoplasmic dynein binds dynactin through a direct interaction between the intermediate chains and p150Glued. J. Cell Biol. 1995; 131:1507–1516. [PubMed: 8522607]
21. Waterman-Storer CM, Karki S, Holzbaur EL. The p150Glued component of the dynactin complex binds to both microtubules and the actin-related protein centractin (Arp-1). Proc. Natl Acad. Sci. USA. 1995; 92:1634–1638. [PubMed: 7878030]
22. Antonny B, Madden D, Hamamoto S, Orci L, Schekman R. Dynamics of the COPII coat with GTP and stable analogues. Nature Cell Biol. 2001; 3:531–537. [PubMed: 11389436]
23. Tang BL, et al. Mammalian homologues of yeast sec31p. An ubiquitously expressed form is localized to endoplasmic reticulum (ER) exit sites and is essential for ER-Golgi transport. J. Biol. Chem. 2000; 275:13597–13604. [PubMed: 10788476]
24. Lowe M, Kreis TE. *In vivo* assembly of coatomer, the COP-I coat precursor. J. Biol. Chem. 1996; 271:30725–30730. [PubMed: 8940050]
25. Echeverri CJ, Paschal BM, Vaughan KT, Vallee RB. Molecular characterization of the 50-kD subunit of dynactin reveals function for the complex in chromosome alignment and spindle organization during mitosis. J. Cell Biol. 1996; 132:617–633. [PubMed: 8647893]
26. Burkhardt JK, Echeverri CJ, Nilsson T, Vallee RB. Overexpression of the dynamitin (p50) subunit of the dynactin complex disrupts dynein-dependent maintenance of membrane organelle distribution. J. Cell Biol. 1997; 139:469–484. [PubMed: 9334349]
27. Quintyne NJ, et al. Dynactin is required for microtubule anchoring at centrosomes. J. Cell Biol. 1999; 147:321–334. [PubMed: 10525538]
28. Vaughan KT, Tynan SH, Faulkner NE, Echeverri CJ, Vallee RB. Colocalization of cytoplasmic dynein with dynactin and CLIP-170 at microtubule distal ends. J. Cell Sci. 1999; 112:1437–1447. [PubMed: 10212138]
29. Holleran EA, Tokito MK, Karki S, Holzbaur EL. Centractin (ARP1) associates with spectrin revealing a potential mechanism to link dynactin to intracellular organelles. J. Cell Biol. 1996; 135:1815–1829. [PubMed: 8991093]
30. Shima DT, Scales SJ, Kreis TE, Pepperkok R. Segregation of COPI-rich and anterograde-cargo-rich domains in endoplasmic-reticulum-to-Golgi transport complexes. Curr. Biol. 1999; 9:821–824. [PubMed: 10469566]
31. Allan BB, Moyer BD, Balch WE. Rab1 recruitment of p115 into a cis-SNARE complex: programming budding COPII vesicles for fusion. Science. 2000; 289:444–448. [PubMed: 10903204]
32. Miller EA, et al. Multiple cargo binding sites on the COPII subunit Sec24p ensure capture of diverse membrane proteins into transport vesicles. Cell. 2003; 114:497–509. [PubMed: 12941277]

33. Mossessova E, Bickford LC, Goldberg J. SNARE Selectivity of the COPII Coat. Cell. 2003; 114:483–495. [PubMed: 12941276]

Europe PMC Funders Author Manuscripts

Europe PMC Funders Author Manuscripts

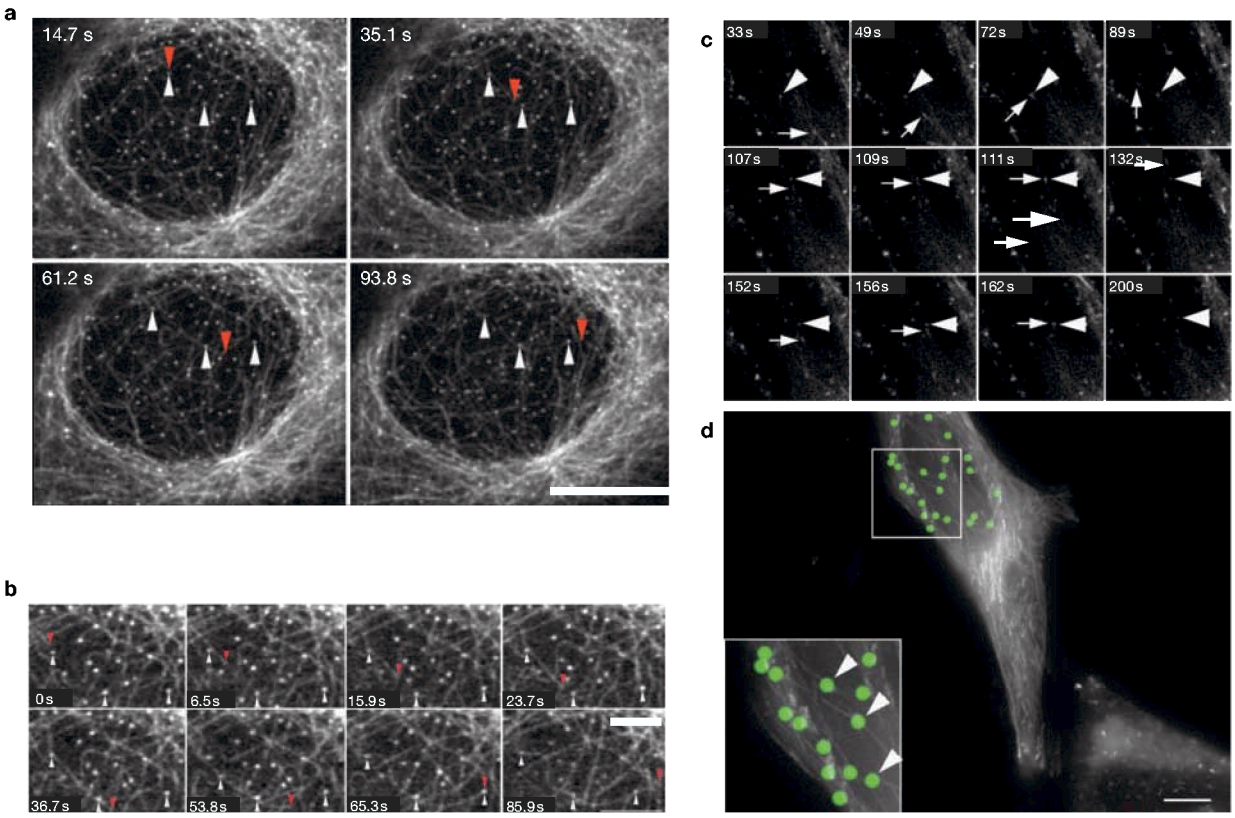

Figure 1.

ERES associate with microtubules and GFP–p150^{Glued}. (**a**) Vero cells expressing Sec23Ap–YFP were microinjected with rhodaminetubulin and imaged after at least 1 h of incubation at 37 °C. The four images show different time points of a time-lapse sequence, in which ERES become rapidly associated with a growing microtubule. The tip of the growing microtubule is highlighted with red arrowheads. ERES that become associated with it are highlighted with white arrowheads. Scale bar, 10 μm; see Supplementary Information, Movie 1. (**b**) Magnification of images at various time points of the time-lapse shown in **a**. Scale bar, 3 μm. (**c**) HeLa cells expressing GFP–p150^{Glued} and GFP–Sec23Ap were imaged at 37 °C. GFP–p150^{Glued} predominantly labels the growing tips of microtubules (arrows), which can be seen to track through the cytoplasm directly through GFP–Sec23Ap-labelled ERES (arrowheads); see Supplementary Information, Movies 2 and 3. (**d**) Maximum intensity projections of all frames from the time-lapse sequence shown in **c**. ERES are pseudo-coloured with green circles; continuous tracks of GFP–p150^{Glued} reveal the paths taken by polymerizing microtubules, which can be seen to grow directly through ERES (arrowheads).

Europe PMC Funders Author Manuscripts
Europe PMC Funders Author Manuscripts

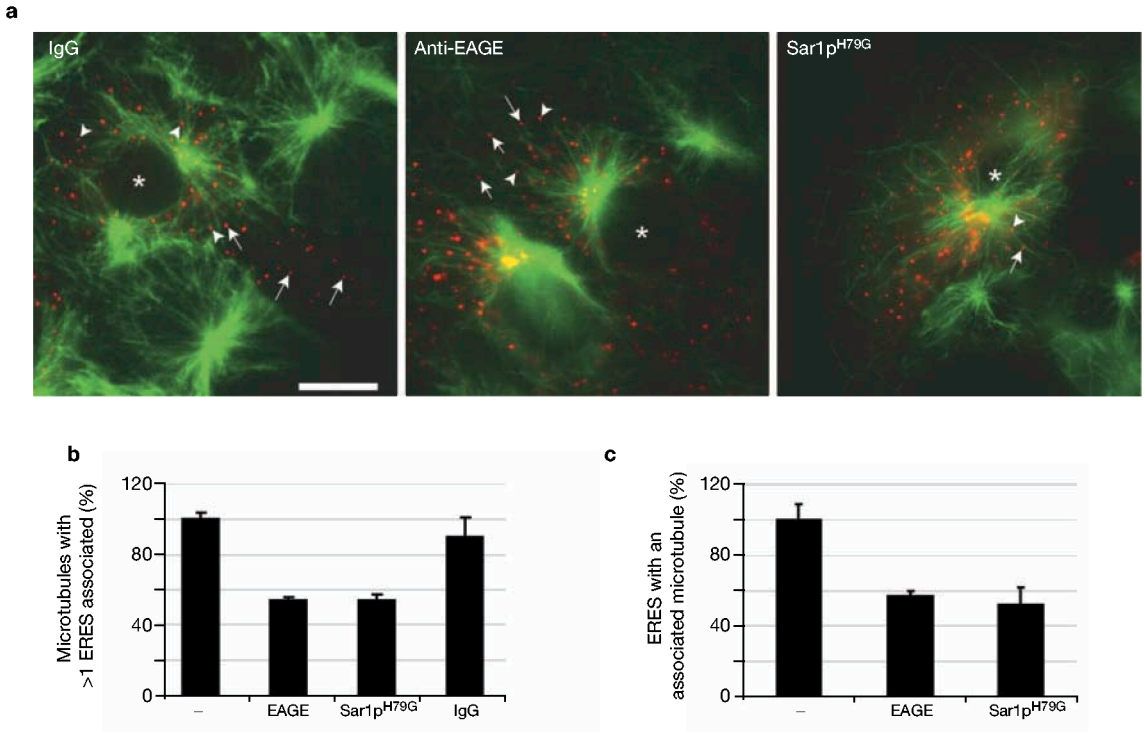

Figure 2.

ERES associate with growing microtubules. (**a**) Association of ERES with newly polymerized microtubules (green) following nocodazole washout. Vero cells expressing YFP–Sec23Ap (red) were microinjected with 1 mg ml−1 rabbit IgG or 1 mg ml−1 anti-EAGE, each with a co-injection marker of 0.03 mg ml−1 rhodamine-dextran to identify injected cells. Sar1p(H79G) was expressed by co-transfection from a plasmid. Depolymerization of microtubules, nocodazole washout, immunostaining of microtubules and determination of the association of COPII-labelled ERES with microtubules was performed as described in Methods. Arrows point to ERES that were considered not to be associated with microtubules, and arrowheads point to ERES that were associated. Scale bar (all panels), 20 μm. (**b**) Quantification of the fraction of microtubules associated with at least one COPII-labelled ERES. (**c**) Quantification of the fraction of COPII-labelled ERES associated with at least one microtubule. Error bars represent s.e.m.

Europe PMC Funders Author Manuscripts
Europe PMC Funders Author Manuscripts

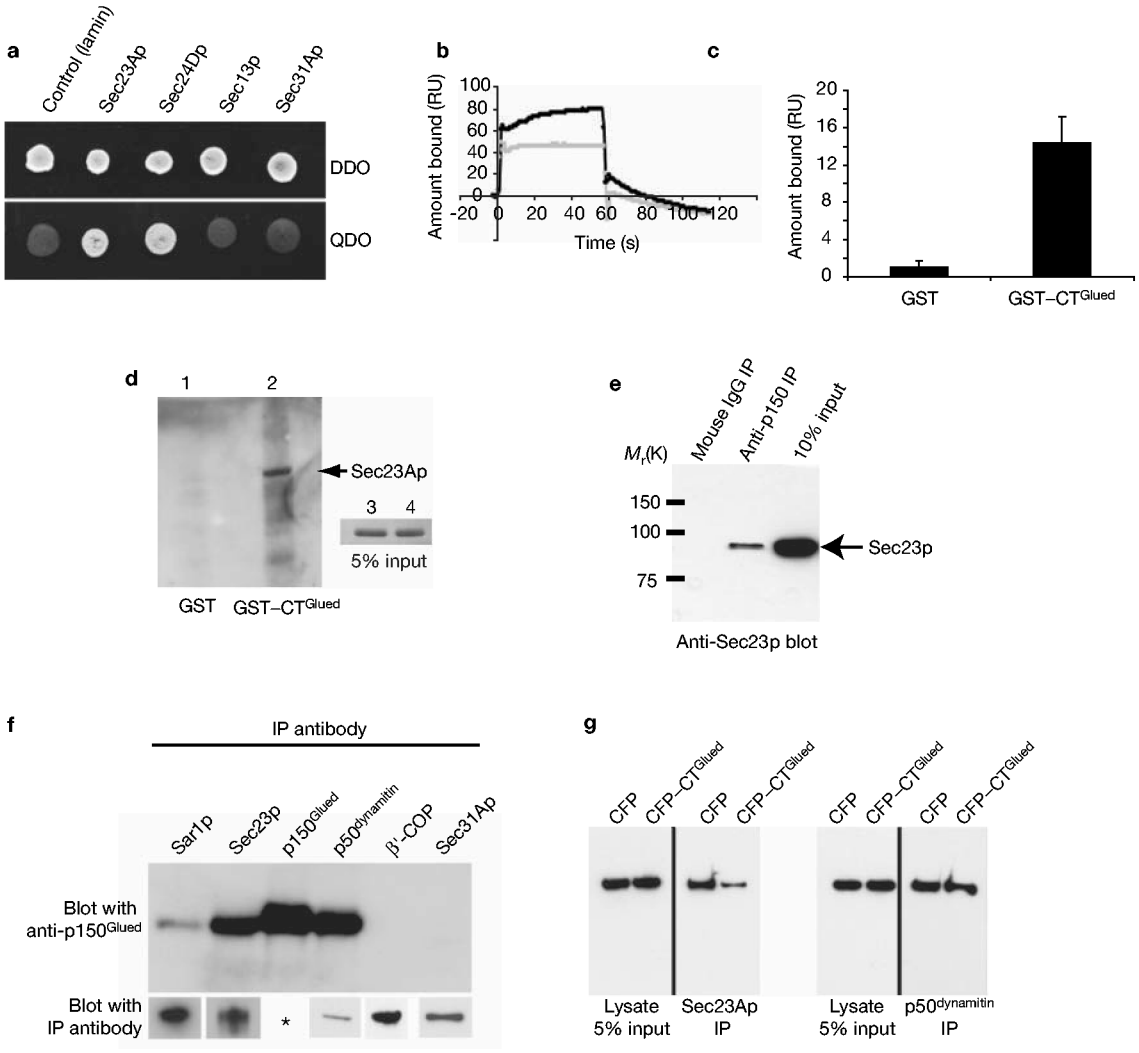

Figure 3.

Interaction of Sec23Ap and p150^{Glued}. (**a**) Two-hybrid screening reveals a specific interaction between Sec23Ap and the C terminus of p150^{Glued} (amino acids 938–1254). All colonies grow on double dropout medium (DDO) but only those showing a positive interaction grow on quadruple dropout (QDO). p150^{Glued} (amino acids 938–1254) interacts specifically with Sec23Ap and Sec24Dp but not with lamin, Sec13p or Sec31Ap. (**b**) Surface plasmon resonance demonstrates a direct interaction between Sec23Ap and p150^{Glued}. One hundred resonance units (RUs) of either GST or GST–CT^{Glued} were immobilized. His$_6$-hSec23Ap shows no binding to GST (grey) but binds GST–CT^{Glued} (black). Note the large increase in RUs immediately following injection of His$_6$-hSec23Ap (t = 0 s) is due to slight differences in refractive indices of the buffers; RUs increase as His$_6$-hSec23Ap flows across the surface loaded with GST–CT^{Glued} but not that loaded with GST. At t = 60 s His$_6$-hSec23Ap is exchanged for PBS. Fast dissociation of His$_6$-hSec23Ap (t = 60 s) is followed by slow dissociation of a more tightly bound component (60–120 s). (**c**) Histogram showing binding of His$_6$-hSec23Ap to GST or GST–CT^{Glued} from six separate experiments. Error bars show ± 1 standard deviation. (**d**) Direct binding of purified His$_6$-Sec23Ap to GST–CT^{Glued}. 5 μg of immobilized GST (lane 1) or GST–CT^{Glued} (lane 2) were incubated with His$_6$-Sec23Ap for 2 h at 4 °C. After washing, proteins were separated and immunoblotted with anti-Sec23Ap. The inset panel shows 5% of the input His$_6$-

Europe PMC Funders Author Manuscripts
Europe PMC Funders Author Manuscripts

Sec23Ap. (**e**) Co-immunoprecipitation of Sec23Ap and $p150^{Glued}$ from HeLa cell lysates. No interaction was detected following immunoprecipitation (IP) with mouse IgG (lane 1) or rabbit IgG (not shown). Interaction was detected following immunoprecipitation of $p150^{Glued}$ and immunoblotting of Sec23Ap (lane 2). Lane 3 shows 10% of the lysate's input. (**f**) $p150^{Glued}$ is immunoprecipitated with antibodies specific for Sar1p and Sec23Ap, as well as $p50^{dynamitin}$ and $p150^{Glued}$ itself. Co-immunoprecipitation is not seen with antibodies specific to β′-COP or Sec31Ap. Efficacy of antibodies in immunoprecipitation was confirmed by immunoblotting with the same antibody (lower panel). Asterisk: specific immunoprecipitation of $p150^{Glued}$ is shown in the top panel. (**g**) Expression of $CFP–CT^{Glued}$ reduces the amount of $p150^{Glued}$ that can be co-immunoprecipitated with Sec23Ap (left-hand panels) but does not affect co-immunoprecipitation of $p150^{Glued}$ with $p50^{dynamitin}$ (right-hand panels).

Europe PMC Funders Author Manuscripts

Europe PMC Funders Author Manuscripts

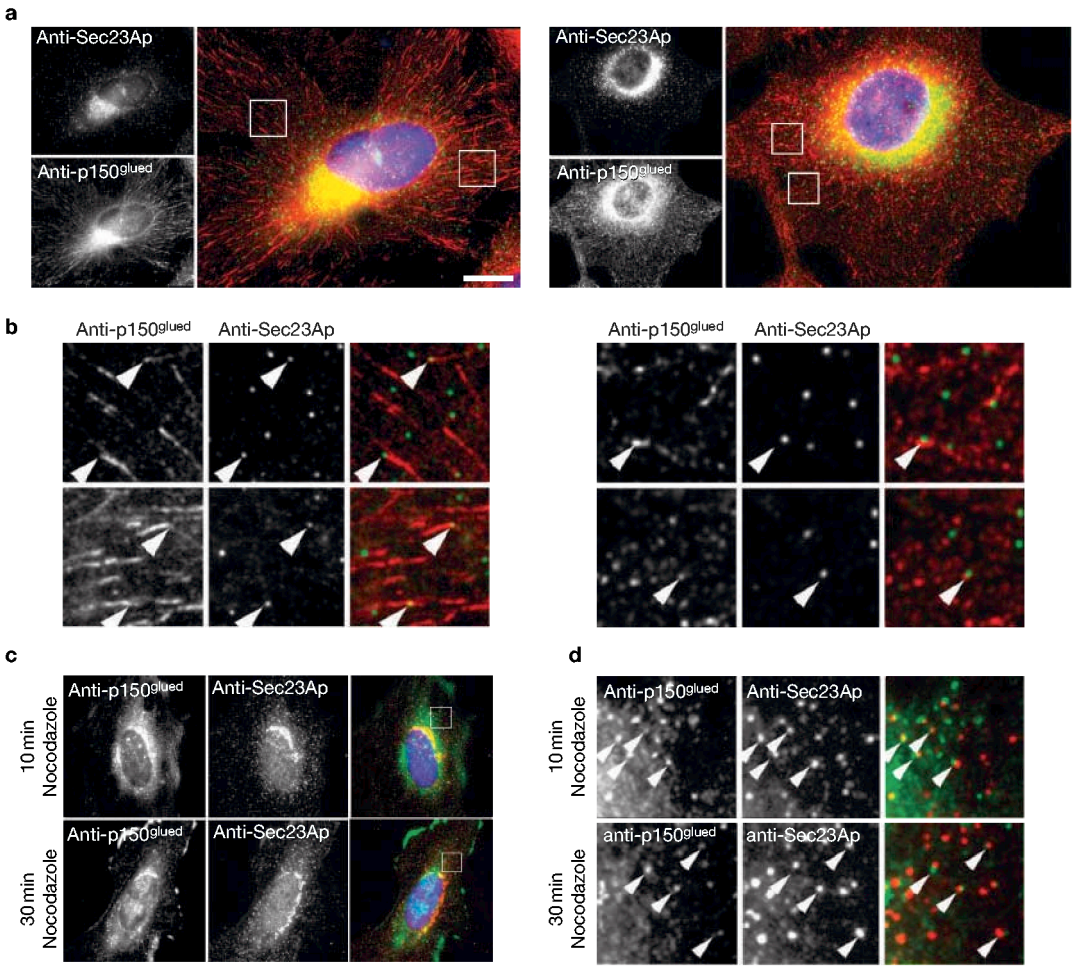

Figure 4.

Colocalization of COPII and p150^{Glued}. (**a**) HeLa cells labelled with antibodies directed against Sec23Ap (top left and green in merge) and two different monoclonal antibodies directed against p150^{Glued} (bottom left and red in merge), followed by DAPI counterstaining of DNA (blue in merge). Scale bar, 5 μm. (**b**) Enlargements of **a** showing (arrowheads) colocalization of Sec23Ap (green) and p150^{Glued} (red) in HeLa cells at steady state. Regions shown are 10 × 10 μm. (**c**) After either a 10 min or 30 min incubation with nocodazole, cells were fixed and processed for immunofluorescence with antibodies directed against Sec23Ap and either α-tubulin or p150^{Glued}. (**d**) Enlargements of the boxed regions in the merge images from **c** highlighting colocalization of Sec23Ap and p150^{Glued} (arrowheads). Quantification of these experiments shows no difference in the degree of colocalization of ERES with p150^{Glued}, either in the presence or absence of microtubules.

Europe PMC Funders Author Manuscripts
Europe PMC Funders Author Manuscripts

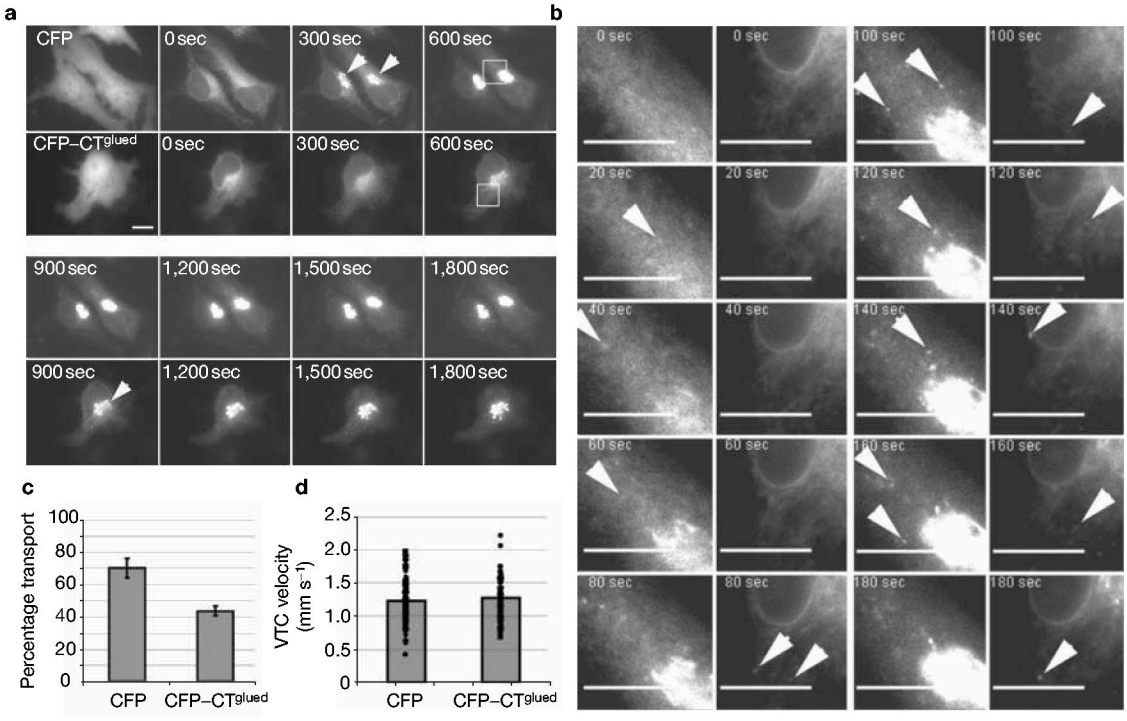

Figure 5.

Expression of the C-terminal 317 amino acids of p150^{Glued} (CT^{Glued}) inhibits cargo export from the ER. (**a**) Cells were transfected with ts045-G–GFP and either CFP or CFP–CT^{Glued} and grown at 39.5 °C for 16 h followed by incubation at 32 °C. The first panels show the expression of CFP and CFP–CT^{Glued}. Subsequent panels show stills from the associated time-lapse movie (see Supplementary Information, Movie 4) taken at the times indicated. Note the substantial localization of ts045-G–YFP to a juxtanuclear (Golgi) region at 300 s in control cells (arrowheads), which does not occur until 900 s in CFP–CT^{Glued}-expressing cells. (**b**) Enlargements of the boxed regions (600 s) in **a** showing localization of ts045-G–YFP at time points indicated). Analysis of the first 3 min of these time-lapse movies shows that the formation of VTCs is delayed in cells expressing CFP–CT^{Glued} (see also Movies 4 and 5, available as Supplementary Information). Later time points reveal the delay in formation of punctate structures (ERES and VTCs, arrowheads). VTCs do form in CFP–CT^{Glued}-transfected cells but their appearance is significantly delayed. (**c**) Quantitative analysis of delivery of ts045-G–YFP to the plasma membrane shows a significant lag in transport in cells co-expressing CFP–CT^{Glued}. The cell surface fluorescence intensity was measured using immunofluorescence of fixed, but nonpermeabilized, cells and normalized to the amount of ts045-G–YFP at the cell surface at 90 min (a measure of the total ts045-G–YFP). Error bars show ±1 s.d.; $P < 0.05$; $n = 3$ experiments, total 30 cells per experiment. (**d**) Velocities of individual VTCs were tracked in cells between 0 and 600 s after shift to 32 °C. The histogram shows the average velocities along with the scatter of individual particle velocities (>100 clearly definable VTCs; at least 20 from each of 5 different cells).

Europe PMC Funders Author Manuscripts
Europe PMC Funders Author Manuscripts